

# Optomechanical control of stacking patterns of h-BN bilayer

Haowei Xu<sup>1</sup>, Jian Zhou<sup>2</sup>, Yifei Li<sup>3</sup>, Rafael Jaramillo<sup>3</sup>, and Ju Li<sup>1,3</sup> (✉)

<sup>1</sup> Department of Nuclear Science and Engineering, Massachusetts Institute of Technology, Cambridge, MA 02139, USA

<sup>2</sup> Center for Advancing Materials Performance from the Nanoscale, State Key Laboratory for Mechanical Behavior of Materials, Xi'an Jiaotong University, Xi'an 710049, China

<sup>3</sup> Department of Materials Science and Engineering, Massachusetts Institute of Technology, Cambridge, MA 02139, USA

© Tsinghua University Press and Springer-Verlag GmbH Germany, part of Springer Nature 2019

Received: 6 June 2019 / Revised: 29 July 2019 / Accepted: 6 August 2019

## ABSTRACT

Few-layer two-dimensional (2D) materials usually have different (meta)-stable stacking patterns, which have distinct electronic and optical properties. Inspired by optical tweezers, we show that a laser with selected frequency can modify the generalized stacking-fault energy landscape of bilayer hexagonal boron nitride (BBN), by coupling to the slip-dependent dielectric response. Consequently, BBN can be reversibly and barrier-freely switched between its stacking patterns in a controllable way. We simulate the dynamics of the stacking transition with a simplified equation of motion and demonstrate that it happens at picosecond timescale. When one layer of BBN has a nearly-free surface boundary condition, BBN can be locked in its metastable stacking modes for a long time. Such a fast, reversible and non-volatile transition makes BBN a potential media for data storage and optical phase mask.

## KEYWORDS

phase change materials, two-dimensional materials, opto-mechanics, density functional theory

Electronic and optical properties of few-layer two-dimensional (2D) materials (e.g., graphene [1–5], hexagonal boron nitride (h-BN) [6–8], transition metal dichalcogenides [9–11] and their heterostructures [12–16]) are strongly affected by their stacking patterns. Some exotic properties are present only for certain stacking modes [17, 18]. For instance, trilayer graphene in ABA (Bernal) stacking is semi-metallic irrespective of external field; while the semi-metallic ABC (rhombohedral) stacking opens a sizable band gap upon applying a gate voltage [1–5]. It is thus highly desirable to be able to change the stacking mode dynamically in a controllable way.

Here, we focus on a robust air-stable 2D material, h-BN, which is an insulator with a wide band gap around 6 eV [6, 19]. Geometrically speaking, the bilayer h-BN (BBN) has five different high symmetry stacking configurations. Among them, AA' (eclipsed with B over N and N over B), A'B (staggered with N over N) and AB' (staggered with B over B) differ only by a translational sliding  $u$  along the armchair direction (Fig. 1). Using first-principles density functional theory (DFT) calculations (see section 4 Methods), we theoretically and computationally demonstrate that the relative stability of these stacking patterns can be effectively tuned by applying a linearly polarized laser (LPL) pulse with selected near-band-edge-transition frequency. Stacking pattern change corresponds to a slippage of the top layer h-BN with respect to the bottom layer. Since the two layers are coupled by weak van der Waals (vdW) interactions, have a small total mass, and are almost unconstrained to the surrounding by long-range elasticity in both  $z$  and  $x, y$  directions (compared to martensitic transformations inside three-dimensional (3D) materials), this stacking change can occur very fast (within picoseconds). Furthermore, such a stacking mode change does not involve any primary bond breaking or reforming, guaranteeing the reversibility.

If BBN has a nearly-free surface boundary to remove tensile strain induced by stacking incommensurability, it can be locked in its metastable stacking modes for a long time, making the switching non-volatile.

We use a non-dimensionalized displacement parameter  $u$  (mod 1) to denote these patterns. The AA' configuration is defined as  $u = 0$ , and the A'B and AB' configurations are  $u = 1/3$  and  $u = 2/3$ , respectively. Note that the other two high symmetry stacking modes, AA (eclipsed with B over B and N over N) and AB (staggered) need a  $\pi/3$  rotation along the  $c$  axis and will be discussed elsewhere.

We begin our discussions with the generalized stacking fault (GSF) [20, 21] energy landscape along the sliding path calculated by DFT [22, 23] with semi-empirical long-range interaction corrections (see section 4 Methods). As shown in Fig. 2(a), AA' is the ground state with lowest energy and is set as the energy reference. The metastable AB' has an energy of 2.1 meV per unit cell (each unit cell contains 4 atoms) higher than that of AA'. Between AA' and AB', there are two barriers on two opposite directions. On the direction that directly links AA' to AB', the A'B stacking serves as the transition saddle-point, 17 meV per unit cell higher in energy than that of AA'. On the opposite direction, there is another barrier at  $u \approx 0.8$  (denoted as saddle-point barrier (SD)), which is 3.0 meV (0.9 meV) per unit cell higher in energy than that of AA' (AB'). These results are consistent with experimental observations that AA' stacking is more often seen than the AB' stacking in clean samples [8, 24].

With external laser illumination, it is possible to tune the relative stability of these high symmetry stacking modes and switch them in a reversible and reduced-energy-barrier (even barrier-free) way. In the following, we will analyze the effect of an LPL with in-plane polarization. In this paper, we do not treat the case of out-of-plane

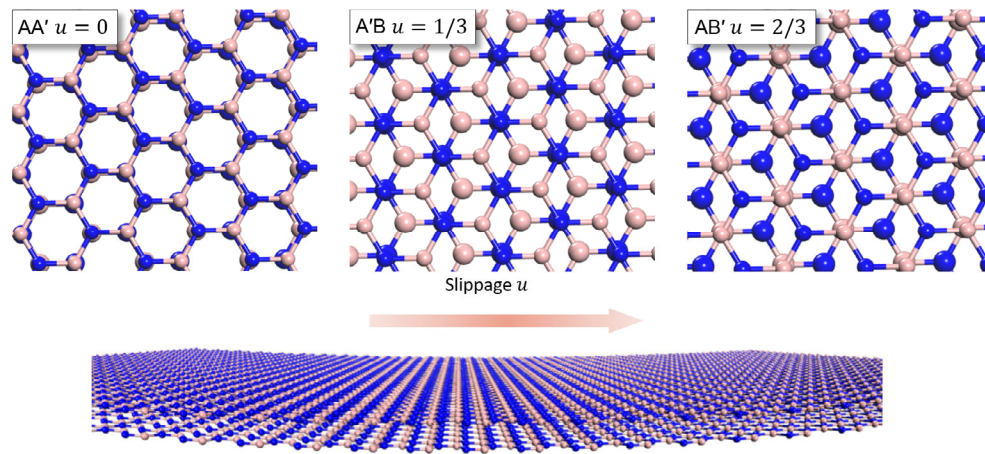


**Figure 1** Three high symmetry stacking modes AA', A'B and AB' of BBN. They are different by a translational sliding  $u$  along the armchair direction (red arrow). AA', A'B and AB' correspond to  $u = 0, 1/3$  and  $2/3$ , respectively. Blue: N; light pink: B. Smaller (larger) atoms lie in the upper (lower) layer.

electric field (gate voltage). Under an electric field  $E$  alternating with frequency  $\omega$ , the free energy per unit cell can be written as [25]

$$\mathcal{G}(u | E, \omega) = \mathcal{G}(u | E = 0) - VE \cdot P_0(u) - \frac{V\epsilon_0}{2} E \cdot \epsilon^{(1)}(u, \omega) \cdot E \quad (1)$$

where  $P_0(u)$  is the intrinsic static polarization density, and  $\epsilon^{(1)}(u, \omega)$  is the real part of dielectric function of a BBN unit cell with displacement  $u$ .  $V$  is the volume of the unit cell. The mechanical work contribution (due to transformation strain) is zero with a slightly pre-buckled, freely suspended boundary condition. At zero temperature,  $\mathcal{G}(u | E = 0)$  is equivalent to the stacking energy per unit cell as shown in Fig. 2(a). The second term, which is the first order response to electric field, averages to be zero when the oscillation frequency  $\omega$  of the electric field is much greater than the phonon vibrational frequency (usually a few THz). The third term is the second order response to the electric field. The dielectric function  $\epsilon(u, \omega)$  should combine the contributions from both ion and electron subsystem. However, the ion subsystem is too sluggish to follow an ultraviolet laser's electric field, so only the contribution from electron subsystem [ $\epsilon(u, \omega) = \epsilon_{\text{electron}}(u, \omega)$ ] is considered in this work. One notable feature of  $\epsilon(u, \omega)$  is that it depends on both the displacement  $u$  and the laser frequency  $\omega$ : the structure determines the dielectric response. Therefore, by careful selection of  $\omega$ , it is possible to modify GSF energy landscape  $\mathcal{G}(u | E, \omega)$ , and effectively tune the relative stability of different stacking configurations.

We calculate  $\epsilon^{(1)}(u, \omega)$  with DFT (see section 4 Methods and the Electronic Supplementary Material (ESM)). Since we consider an LPL polarized in the  $x$  direction, the only contribution to the total free energy is the  $\epsilon_{xx}$  term.  $\epsilon_{xx}^{(1)}(u, \omega)$  for  $\omega$  from 4.0 to 6.5 eV is plotted in Fig. 2(b). We can see that in this frequency range,  $\epsilon_{xx}^{(1)}(u, \omega)$  is sensitive to both  $u$  and  $\omega$ . For  $\omega < 4.0$  eV, which is below the band edge,  $\epsilon_{xx}^{(1)}(u, \omega)$  is nearly constant for all  $u$ . This can be understood from the

$$\text{Kramers-Kronig relation } \epsilon_{\alpha\beta}^{(1)}(u, \omega) = 1 + \frac{2}{\pi} P \int_0^\infty \frac{\epsilon_{\alpha\beta}^{(2)}(u, \omega') \omega'}{\omega'^2 - \omega^2 + i\eta} d\omega'.$$

For  $\omega$  well below the bandgap,  $\epsilon_{\alpha\beta}^{(2)}(u, \omega)$  is close to zero for all  $u$ , thus  $\epsilon_{\alpha\beta}^{(1)}(u, \omega)$  is nearly a constant. But for  $\omega$  close to the band edge transition frequency, since the stacking pattern  $u$  has an influence on the electronic band structure [6],  $\epsilon_{\alpha\beta}^{(2)}(u, \omega)$  would be different for different  $u$ , which in turn leads to the strong dependence of  $\epsilon_{\alpha\beta}^{(1)}(u, \omega)$  on  $u$ .  $\epsilon_{xx}^{(1)}(u, \omega)$  at two selected frequencies,  $\omega = 4.30$  and 4.55 eV are shown in Fig. 2(c). For  $\omega = 4.30$  eV,  $\epsilon_{xx}^{(1)}(AB')$  is 10.9, greater than both  $\epsilon_{xx}^{(1)}(AA')$  (8.92) and  $\epsilon_{xx}^{(1)}(SD)$  (9.87). Therefore, when a LPL polarized in the  $x$ -direction with  $\omega = 4.30$  eV is applied,  $\mathcal{G}(AB')$  would get relatively lower in the GSF energy. When the laser is strong enough ( $E > 1.8$  V/nm), AB' stacking can be the most

stable, with  $\mathcal{G}(AB') < \mathcal{G}(AA')$ . In this case, BBN originally at AA' stacking may slip into AB' stacking, aided by the nucleation of a partial dislocation loop. This effect is shown in Fig. 2(d). In order to induce a barrier-free transition, the minimum alternating electric field strength is  $E = 3.5$  V/nm (corresponds to laser pulse intensity  $I_0 = 1.6 \times 10^{12}$  W/cm<sup>2</sup>).

Once the laser is turned off, the BBN at AB' stacking has the thermodynamic driving force to return to AA' because AA' stacking is lower in energy without laser illumination. However, such a transition is hindered by the SD between AA' and AB' and a domain may be locked in AB' for a very long time before collectively transiting back to AA', provided that the boundary condition is set right, namely to let the dislocation loop merge into the vacuum and "disappear", rather than piling up at the edges, during writing. In this case the transition rate can be estimated as  $\Gamma = \nu_0 \exp\left(-\frac{N\Delta\mathcal{G}}{k_B T}\right)$ ,

where  $\nu_0$  is the trial frequency and is usually at the order of  $10^{12}$  s<sup>-1</sup>,  $N$  is the number of the unit cells and  $\Delta\mathcal{G}$  is the height of the barrier (0.9 meV here). We can see that even if  $N = 2,000$ , the collective transition would take  $10^{12}$  years at the room temperature. However, if there is no barrier in the landscape, BBN would transit freely from AB' to AA' and as we will elaborate later, the transition time is at the order of ps. In order to trigger such an instantaneous and fast transition from AB' to AA', a laser with frequency  $\omega = 4.55$  eV can be applied. We also plot calculated  $\epsilon_{xx}^{(1)}(u, \omega = 4.55$  eV) in Fig. 2(c). It demonstrates an order of dielectric function  $\epsilon_{xx}^{(1)}(SD) > \epsilon_{xx}^{(1)}(AA') > \epsilon_{xx}^{(1)}(AB')$ . When the laser with electric field strength  $E$  greater than 1.0 V/nm is applied, the desired grand potential order  $\mathcal{G}(AB') > \mathcal{G}(SD) > \mathcal{G}(AA')$  can be obtained, enabling a barrier-free transition from AB' to AA'. These alternating electric field magnitudes are moderate and achievable in current experiments.

Next, we explore the dynamics of such transition with a one-dimensional (1D) equation of motion. As shown in Fig. 2(e), the model consists 2 layers of particles, each particle represents a unit cell in one layer, and is indexed by  $n$  ranging in  $1, 2, \dots, N$ . For simplicity, the positions of particles on the bottom layer are fixed as reference points. Particles on the top layer are allowed to move and their configuration are described by the displacements  $\{u_n, n = 1, 2, \dots, N\}$  relative to the particles on the bottom layer. Three independent interactions are accounted, namely,  $U_{\text{elastic}} + U_{\text{vdW}} + U_E$ . The first one is the intra-plane interaction on the top layer, which is approximated by a harmonic spring with elastic constant  $\kappa$ . The second term is the vdW interaction  $U_{\text{vdW}}$  between the two layers. The third interaction is the interaction under the laser field  $U_E$ , which is determined by the BBN slip-dependent dielectric function

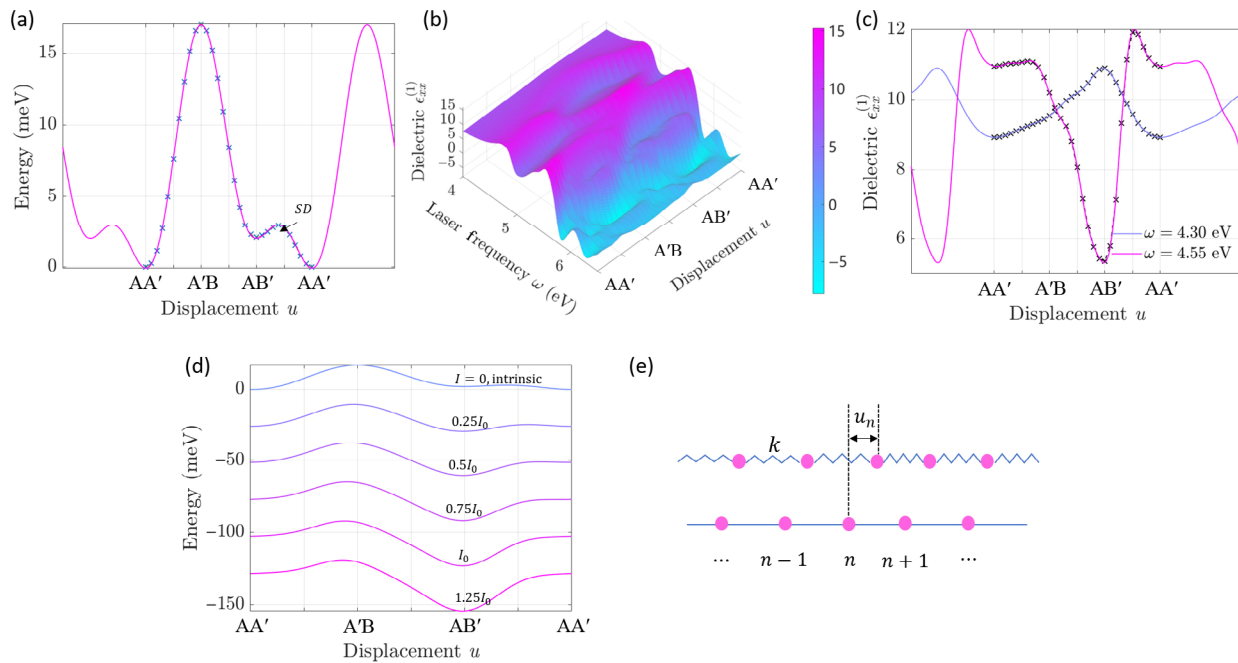


**Figure 2** (a) Intrinsic BBN GSF energy landscape along the armchair direction. Three high symmetry stacking modes are labeled. AA' is stable, AB' is metastable, and A'B is unstable. SD denotes the saddle point between AA' to AB'. AA' is set as the energy reference in the plot. (b) Calculated dielectric function  $\epsilon_{xx}^{(1)}(u, \omega)$  for  $\omega$  from 4.0 to 6.5 eV. (c) Dielectric function  $\epsilon_{xx}^{(1)}(u, \omega)$  at two selected frequencies  $\omega = 4.30$  and 4.55 eV.  $\epsilon_{xx}^{(1)}(u)$  at a fixed frequency is dependent on the displacement  $u$  and can tune the shape of stacking energy landscape  $\mathcal{G}(u)$ .  $\omega = 4.30$  eV favors AB' stacking while  $\omega = 4.55$  eV favors AA' stacking. In (a) and (b), crosses are from DFT calculations while solid curves are Fourier series fittings. (d) GSF energy  $\mathcal{G}(u, \omega = 4.30$  eV) at several different laser intensity.  $I_0$  corresponds to  $E_0 = 3.5$  V/nm and is strong enough to induce barrier free transition from AA' to AB'. (e) The 1D model system as described in the main text. Each pink point represents a unit cell on one layer.

(see Eq. (1)). Now we can put all ingredients together and write down the Lagrangian  $\mathcal{L}$  of the system

$$\mathcal{L} = \int dt \sum_{n=1}^N \left[ \frac{ma^2}{2} \left( \frac{\partial u_n}{\partial t} \right)^2 - \frac{\kappa a^2}{2} \frac{1}{2} [(u_{n+1} - u_n)^2 + (u_n - u_{n-1})^2] - U_{\text{vdw}}(u_n) + \frac{\epsilon(u_n) \epsilon_0 V}{2} E^2(n) \right] \quad (2)$$

By applying Lagrange's equation, we can derive the equation of motion (EOM) for the  $n$ -th particle on the top layer

$$\frac{\partial^2 u_n}{\partial t^2} = \frac{\kappa}{m} (u_{n+1} + u_{n-1} - 2u_n) - \frac{1}{ma^2} \left[ \frac{\partial U_{\text{vdw}}(u_n)}{\partial u_n} - \frac{\epsilon_0 V E^2(n)}{2} \frac{\partial \epsilon(u_n)}{\partial u_n} \right] - \gamma \frac{\partial u_n}{\partial t} \quad (3)$$

Here,  $m$  is the effective mass of a unit cell ( $m = m_b + m_s$ ),  $a \approx 4.3$  Å is the lattice spacing (along the armchair direction). The elastic constant  $\kappa$  for a flat BBN can be obtained by fitting the strain-energy curve. In order to calculate the derivative of  $U_{\text{vdw}}$  and  $\epsilon$  with respect to  $u$ , we fit them with Fourier series (solid curves in Figs. 2(a) and 2(c)). The last term in Eq. (3) is a damping term, representative of all possible dissipation effects in the system. Considering that the phonon lifetime at room temperature is on the order of ps [26], phonon-phonon scattering would lead to a partial contribution of  $\gamma \sim 1$  ps<sup>-1</sup>. Since there are other contributions to the total dissipation, such as defects and the larger anharmonicity when  $u$  is large, it is reasonable to assume that  $\gamma$  is on the order of several ps<sup>-1</sup>. In general,  $\gamma$  determines how quickly the oscillations around the GSF energy minimum damp out, and in turn determines the transition time. But the main conclusions do not sensitively depend on the specified value of  $\gamma$ . In the following,  $\gamma$  is set as 5 ps<sup>-1</sup>. If a larger  $\gamma$  is used, the dynamics of the system is slower, but the oscillation around the GSF energy minimum is also weaker. On the other hand, if a smaller  $\gamma$  is used, the dynamics becomes faster but the oscillation around

the GSF energy minimum would take more periods to be damped out. This is similar to overdamped, critically damped and underdamped behaviors of a damped oscillator.

We solve EOM Eq. (3) with a total number of unit cells  $N = 20,000$ . The results (Fig. 3) show that AA' and AB' can be switched in picoseconds under laser with selected frequency. In Fig. 3(a), the system is originally in a homogeneous AA' stacking mode (blue curve). By shining laser with frequency  $\omega = 4.30$  eV, and Gaussian profile

$$E(n) = E_0 \exp \left[ -\frac{(n - n_0)^2}{2\sigma^2} \right] \text{ with } E_0 = 5.0 \text{ V/nm, } n_0 = 10,000 \text{ and}$$

$\sigma = 2,000$  (with full width at half maximum around 1  $\mu\text{m}$ , denoted as Laser-A) in the middle region, AB' stacking domain starts to develop. At  $t = 2.5$  ps, Laser-A is turned off and the system is allowed to relax freely. We can see that the middle region of the system first oscillates around AB' stacking, and after the oscillation damps out, it is locked in AB' (yellow curve). The whole process takes about 5 ps. The thickness of the domain wall (DW) between AA' and AB' is about 100 unit cell length, roughly 40 nm. In Fig. 3(b), the system is initially set as the final state of Fig. 3(a). At  $t = 0$ , a laser with frequency  $\omega = 4.55$  eV, and the same profile as Laser-A except that  $E_0 = 1.5$  V/nm (denoted as Laser-B) starts to shine on the AB' domain. At  $t = 0.5$  ps, Laser-B is turned off, and the system automatically collapses back to AA'. The DWs are erased as well and the system is restored to the initial state in Fig. 3(a), leaving no trace. That is, by alternatively applying Laser-A and Laser-B, the AB' stacking domain can be written and erased within picoseconds according to the EOM.

In Figs. 3(c) and 3(d), we show that the DW can be moved towards the AB' (AA') domain by moving Laser-A (Laser-B), with a mechanism similar to writing (erasing) AB' stacking modes. Originally, the system contains a AB' domain, separated from two AA' domains by DWs (oppositely signed dislocations). In Fig. 3(c), by shining Laser-A on the left DW and moving the laser to left, AB'

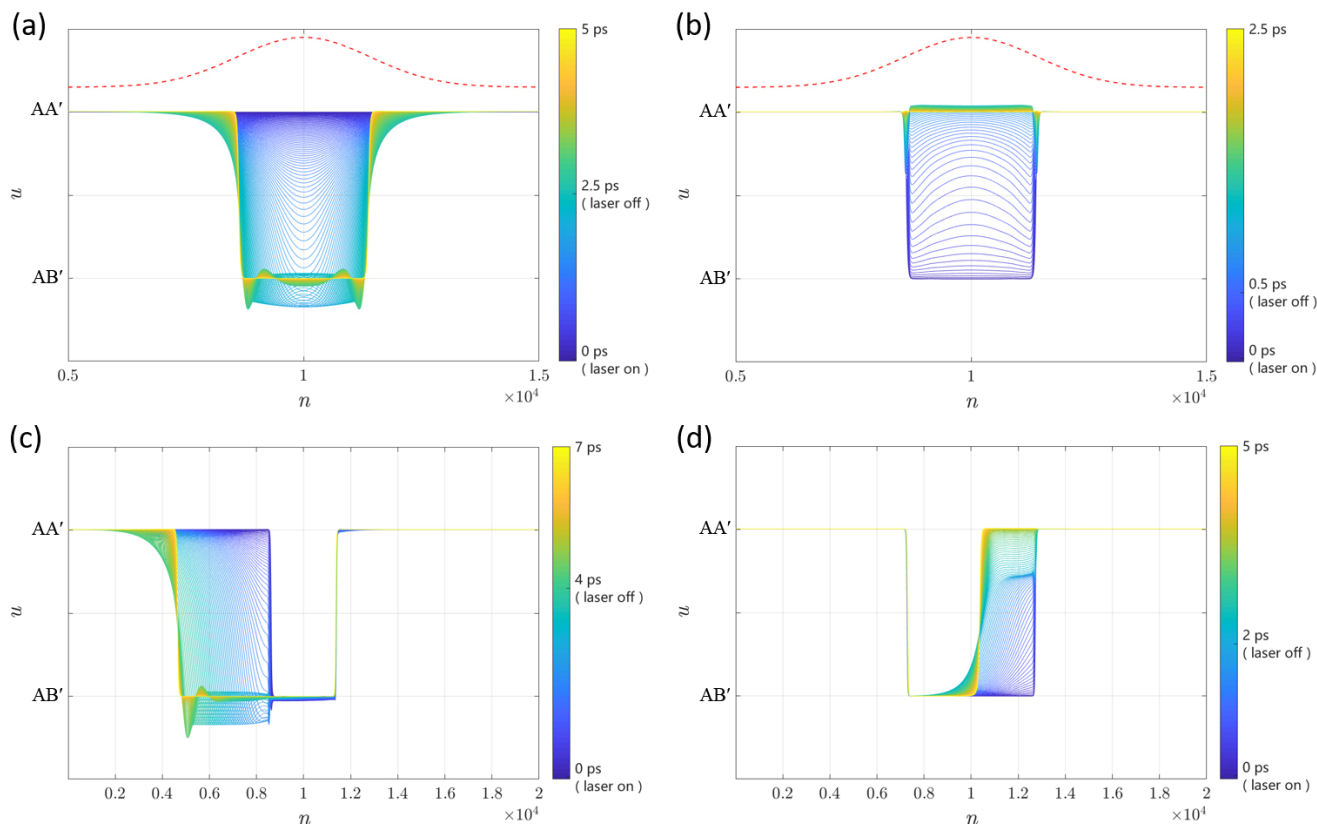


**Figure 3** Dynamics of the model system under different laser illumination. (a) Writing AB' domain. Initially the system is in a homogeneous AA' stacking mode. From  $t = 0$  to 2.5 ps, Laser-A, which favors AB' stacking mode shines on the middle region. An AB' domain gradually develops. After several oscillations, middle region of the system is locked in the AB' stacking mode. (b) Erasing AB' domain. The initial state here is the final state in (a). Between  $t = 0$  to 0.5 ps, Laser-B, which favors AA' stacking mode shines on the AB' domain. The system is restored to the initial state in (a), which is a homogeneous AA' domain. The laser profile is shown as the red dotted lines in (a) and (b). (c) and (d) Moving DW. Laser-A (Laser-B) shines on the DW between AA' and AB' domain, and moves towards AB' (AA') domain. The DW moves in the same direction as the laser.

domain gradually grows to the left, replacing AA' domain. Similarly, in Fig. 3(d), by shining Laser-B on the right DW and moving the laser to the left, AA' domain grows to the left and swallows AB' domain. Both processes happen in picoseconds.

It should be noted that in our spatially extensive model system with finite elastic constant  $\kappa \sim 10 \text{ eV}/\text{\AA}^2$ , AB' domain is not very stable when the laser is turned off. Due to the elastic interaction between neighboring particles within the DW and the intrinsic metastability of AB' stacking mode, AB'-AA' DW would move towards the AB' direction and AB' domain shrinks with time, with a speed on the order of nm/ps. Therefore, a AB' domain with micrometer dimension would disappear in nanoseconds. To make the switching between different stacking modes non-volatile, the long-range elastic interaction in  $x, y$  should be eliminated. Fortunately, the elastic interaction exists only within the DW and can be removed by simply removing the DW (dislocation core). One way is to use a free surface boundary condition, as shown in Fig. 4. Monolayer h-BN flakes with dimension comparable to the spot size of the laser are distributed freely as separate sheets on the bottom layer, each of which can slide in-plane, like an air hockey table. If the spacing between top sheets are large enough and separated by boundary walls, there will be no crosstalk between them. When the laser is focused on one domain, it would transit collectively between AA' and AB' stacking modes. With the new stacking domain growing in size, the bounding partial dislocation loop will eventually be so large that it is pushed to the free boundary and annihilate there, rather than piling up at the boundary wall if both h-BN layers were clamped at the edge. This way, the in-plane elastic interaction can be nearly entirely removed and AB' domain can be locked in for a long time, rendering the switching non-volatile. To switch back, a new laser pulse

has to be applied again, and an entirely new partial dislocation loop needs to nucleate afresh.

Since the switching between different stacking modes is fast, reversible and non-volatile, we suggest that BBN could serve as a data storage media. Compared with currently used phase change materials [27] such as Ge-Sb-Te alloys, which can be switched between crystalline and amorphous phases upon heating over 1–1,000 nanoseconds time scale, the non-volatile phase transition in BBN can be ultrafast, athermal, and displacive. The EOM Eq. (3) has similar structure as the Frenkel-Kontorova model, with external forcing by the optical tweezing, that takes advantage of the significant contrast in dielectric response offered by the slippage.

Based on this discussion, we illustrate a BBN optical disc drive (Fig. 4(b)). It is a lattice of BBN sheets with nearly-free surface boundary condition as describe above. The bottom layer can be deposited as rigid and flat, and can also be lifted off and wrapped as a scroll to increase the volume density for data storage (Fig. 4(b)). Note that the areal data density is limited by the laser spot size, which is in turn limited by the diffraction limit. For the laser used here with incident energy around 4 eV (corresponding to 300 nm wavelength), the diffraction limit is on the order of hundreds of nanometers. This size is also resolvable by imaging systems with optical wavelength of  $\sim 300 \text{ nm}$ . Lasers can move around to read and write. We propose to use high intensity lasers to write and erase AA' (or AB') configuration, which can serve as 0 (or 1) state. For reading, one applies a laser with low intensity, and measures the luminescence, or refractive index by ellipsometry, which are very distinct at certain frequencies for different stacking patterns [8]. Such a BBN disk can be switched back and forth at much faster bitrates of current phase-change storage media.

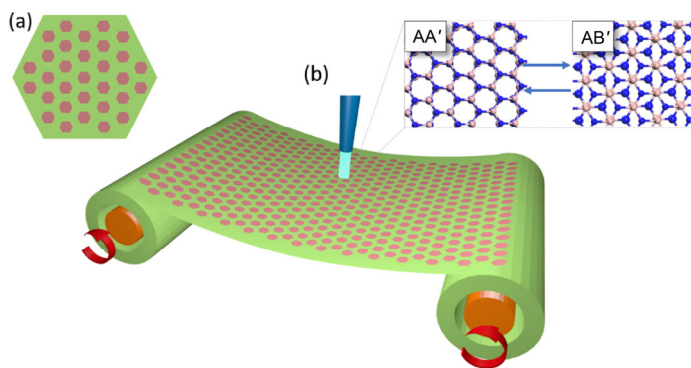


**Figure 4** (a) BBN sheets with nearly-free surface boundary condition. Monolayer h-BN sheets with size comparable to the spot size of the laser are distributed on the the bottom layer. Each domain size is on the order of a few hundred nanometers, owing to the limitation of optical resolution and laser beam width. The top layers can move nearly freely upon laser illumination and BBN sheets can collectively transit between AA' and AB' stacking modes. The dislocation induced is absorbed by the nearly-free boundary. No DW is formed so that the elastic interaction is eliminated and the AB' stacking mode can be locked for a very long time, rendering the switching non-volatile. (b) BBN optical disk drive as a lattice of BBN sheets in (a). BBN layers can be scrolled to increase data density. Laser moves around to read and write.

We would like to make some final remarks. First, such a scheme of optical tweezing is not limited to slippage: the other two high symmetry stacking modes, AA and AB, can come into play as well by twisting. Some experimental and computational works have shown that AB stacking is also stable, with stacking energy comparable to that of AA' [7, 24]. The relative stability between these high symmetry stacking modes may be tuned by laser with selected frequency and polarization. Our model can thus be extended to 2D slippage and twisting. Second, the spatial density of storage can be very high, with locked-in domain as small as tens of nanometers, and by rolling up the 2D material as a scroll akin to DNA packing, one may achieve high total storage density in 3D. Third, besides data storage, optical stacking mode transition may find other applications such as in programmable optical switches, phase masks, grating array, etc. We expect that our theoretical prediction could evoke experimental validations in the near future.

## Methods

Our first-principles calculations are based on DFT [22, 23] as implemented in Vienna *ab initio* simulation package (VASP) [28, 29]. Exchange-correlation interactions are treated by generalized gradient approximation (GGA) of Perdew–Burke–Ernzerhof (PBE) [30] form. Core and valence electrons are treated by projector augmented wave (PAW) method [31] and a plane wave basis set, respectively. The kinetic energy cutoff is set as 400 eV and the first Brillouin zone is sampled by a  $11 \times 11 \times 1$   $\Gamma$ -centered  $k$ -point mesh. Interlayer van der Waals interactions are treated with DFT-D3 method of Grimme with Becke–Johnson damping [32, 33]. For each displacement  $u$ , the in-plane lattice constant is fixed at 2.50 Å but the inter-plane distance is allowed to relax, until forces on all atoms are smaller than 0.001 eV/Å. The dielectric function is calculated in the independent particle approximation (IPA). More accurate quasi-particle GW calculations [34, 35] with exciton binding correction (Bethe–Salpeter equation, BSE [36, 37]) calculations are also performed and the results are qualitatively consistent with IPA results.

## Acknowledgements

This work was supported by an Office of Naval Research MURI through grant #N00014-17-1-2661.

**Electronic Supplementary Material:** Supplementary material (further details on the dynamics of the stacking pattern transition and the dielectric function of BBN) is available in the online version of this article at <https://doi.org/10.1007/s12274-019-2500-y>.

## References

- [1] Guinea, F.; Castro Neto, A. H.; Peres, N. M. R. Electronic states and Landau levels in graphene stacks. *Phys. Rev. B* **2006**, *73*, 245426.
- [2] Aoki, M.; Amawashi, H. Dependence of band structures on stacking and field in layered graphene. *Solid State Commun.* **2007**, *142*, 123–127.
- [3] Craciun, M. F.; Russo, S.; Yamamoto, M.; Oostinga, J. B.; Morpurgo, A. F.; Tarucha S. Trilayer graphene is a semimetal with a gate-tunable band overlap. *Nat. Nanotechnol.* **2009**, *4*, 383–388.
- [4] Koshino, M. Interlayer screening effect in graphene multilayers with ABA and ABC stacking. *Phys. Rev. B* **2010**, *81*, 125304.
- [5] Bao, W.; Jing, L.; Velasco, J. Jr.; Lee, Y.; Liu, G.; Tran, D.; Standley, B.; Aykol, M.; Cronin, S. B.; Smirnov, D. et al. Stacking-dependent band gap and quantum transport in trilayer graphene. *Nat. Phys.* **2011**, *7*, 948–952.
- [6] Marom, N.; Bernstein, J.; Garel, J.; Tkatchenko, A.; Joselevich, E.; Kronik, L.; Hod, O. Stacking and registry effects in layered materials: The case of hexagonal boron nitride. *Phys. Rev. Lett.* **2010**, *105*, 046801.
- [7] Constantinescu, G.; Kuc, A.; Heine, T. Stacking in bulk and bilayer hexagonal boron nitride. *Phys. Rev. Lett.* **2013**, *111*, 036104.
- [8] Bourrellier, R.; Amato, M.; Galvão Tizei, L. H.; Giorgetti, C.; Gloter, A.; Heggie, M. I.; March, K.; Stéphane, O.; Reining, L.; Kociak, M. et al. Nanometric resolved luminescence in h-BN flakes: Excitons and stacking order. *ACS Photonics* **2014**, *1*, 857–862.
- [9] Wilson, J. A.; Yoffe, A. D. The transition metal dichalcogenides discussion and interpretation of the observed optical, electrical and structural properties. *Adv. Phys.* **1969**, *18*, 193–335.
- [10] Eda, G.; Fujita, T.; Yamaguchi, H.; Voiry, D.; Chen, M. W.; Chhowalla, M. Coherent atomic and electronic heterostructures of single-layer MoS<sub>2</sub>. *ACS Nano* **2012**, *6*, 7311–7317.
- [11] Duerloo, K. A. N.; Li, Y.; Reed, E. J. Structural phase transitions in two-dimensional Mo- and W-dichalcogenide monolayers. *Nat. Commun.* **2014**, *5*, 4214.
- [12] Geim, A. K.; Grigorieva, I. V. Van der Waals heterostructures. *Nature* **2013**, *499*, 419–425.
- [13] Novoselov, K. S.; Mishchenko, A.; Carvalho, A.; Castro Neto, A. H. 2D materials and van der Waals heterostructures. *Science* **2016**, *353*, aac9439.
- [14] Woods, C. R.; Britnell, L.; Eckmann, A.; Ma, R. S.; Lu, J. C.; Guo, H. M.; Lin, X.; Yu, G. L.; Cao, Y.; Gorbachev, R. V. et al. Commensurate–incommensurate transition in graphene on hexagonal boron nitride. *Nat. Phys.* **2014**, *10*, 451–456.
- [15] Eckmann, A.; Park, J.; Yang, H. F.; Elias, D.; Mayorov, A. S.; Yu, G. L.; Jalil, R.; Novoselov, K. S.; Gorbachev, R. V.; Lazzeri, M. et al. Raman fingerprint of aligned graphene/h-BN superlattices. *Nano Lett.* **2013**, *13*, 5242–5246.
- [16] An, Y. P.; Zhang, M. J.; Wu, D. P.; Wang, T. X.; Jiao, Z. Y.; Xia, C. X.; Fu, Z. M.; Wang, K. The rectifying and negative differential resistance effects in graphene/h-BN nanoribbon heterojunctions. *Phys. Chem. Chem. Phys.* **2016**, *18*, 27976–27980.
- [17] Qian, X. F.; Liu, J. W.; Fu, L.; Li, J. Quantum spin Hall effect in two-dimensional transition metal dichalcogenides. *Science* **2014**, *346*, 1344–1347.
- [18] Dean, C. R.; Wang, L.; Maher, P.; Forsythe, C.; Ghahari, F.; Gao, Y.; Katoch, J.; Ishigami, M.; Moon, P.; Koshino, M. et al. Hofstadter’s butterfly and the fractal quantum Hall effect in moiré superlattices. *Nature* **2013**, *497*, 598–602.
- [19] Cassabois, G.; Valvin, P.; Gil, B. Hexagonal boron nitride is an indirect bandgap semiconductor. *Nat. Photonics* **2016**, *10*, 262–266.
- [20] Vitek, V. Intrinsic stacking faults in body-centred cubic crystals. *Philos. Mag.* **1968**, *18*, 773–786.
- [21] Ogata, S.; Li, J.; Yip, S. Ideal pure shear strength of aluminum and copper. *Science* **2002**, *298*, 807–811.
- [22] Hohenberg, P.; Kohn, W. Inhomogeneous electron gas. *Phys. Rev.* **1964**, *136*, B864–B871.

- [23] Kohn, W.; Sham, L. J. Self-consistent equations including exchange and correlation effects. *Phys. Rev.* **1965**, *140*, A1133–A1138.
- [24] Warner, J. H.; Rummeli, M. H.; Bachmatiuk, A.; Büchner, B. Atomic resolution imaging and topography of boron nitride sheets produced by chemical exfoliation. *ACS Nano* **2010**, *4*, 1299–1304.
- [25] Zhou, J.; Xu, H. W.; Li, Y. F.; Jaramillo, R.; Li, J. Opto-mechanics driven fast martensitic transition in two-dimensional materials. *Nano Lett.* **2018**, *18*, 7794–7800.
- [26] Cuscó, R.; Artús, L.; Edgar, J. H.; Liu, S.; Cassabois, G.; Gil, B. Isotopic effects on phonon anharmonicity in layered van der Waals crystals: Isotopically pure hexagonal boron nitride. *Phys. Rev. B* **2018**, *97*, 155435.
- [27] Wuttig, M.; Yamada, N. Phase-change materials for rewriteable data storage. *Nat. Mater.* **2007**, *6*, 824–832.
- [28] Kresse, G.; Furthmüller, J. Efficiency of *ab-initio* total energy calculations for metals and semiconductors using a plane-wave basis set. *Comput. Mater. Sci.* **1996**, *6*, 15–50.
- [29] Kresse, G.; Furthmüller, J. Efficient iterative schemes for *ab initio* total-energy calculations using a plane-wave basis set. *Phys. Rev. B* **1996**, *54*, 11169–11186.
- [30] Perdew, J. P.; Burke, K.; Ernzerhof, M. Generalized gradient approximation made simple. *Phys. Rev. Lett.* **1996**, *77*, 3865–3868.
- [31] Blöchl, P. E. Projector augmented-wave method. *Phys. Rev. B* **1994**, *50*, 17953–17979.
- [32] Grimme, S.; Antony, J.; Ehrlich, S.; Krieg, H. A consistent and accurate *ab initio* parametrization of density functional dispersion correction (DFT-D) for the 94 elements H–Pu. *J. Chem. Phys.* **2010**, *132*, 154104.
- [33] Grimme, S.; Ehrlich, S.; Goerigk, L. Effect of the damping function in dispersion corrected density functional theory. *J. Comput. Chem.* **2011**, *32*, 1456–1465.
- [34] Hedin, L. New method for calculating the one-particle green's function with application to the electron-gas problem. *Phys. Rev.* **1965**, *139*, A796–A823.
- [35] Hybertsen, M. S.; Louie, S. G. First-principles theory of quasiparticles: Calculation of band gaps in semiconductors and insulators. *Phys. Rev. Lett.* **1985**, *55*, 1418–1421.
- [36] Salpeter, E. E.; Bethe, H. A. A relativistic equation for bound-state problems. *Phys. Rev.* **1951**, *84*, 1232–1242.
- [37] Onida, G.; Reining, L.; Rubio, A. Electronic excitations: Density-functional versus many-body green's-function approaches. *Rev. Mod. Phys.* **2002**, *74*, 601–659.

# Electronic Supplementary Material

## Optomechanical control of stacking patterns of h-BN bilayer

Haowei Xu<sup>1</sup>, Jian Zhou<sup>2</sup>, Yifei Li<sup>3</sup>, Rafael Jaramillo<sup>3</sup>, and Ju Li<sup>1,3</sup> (✉)

<sup>1</sup> Department of Nuclear Science and Engineering, Massachusetts Institute of Technology, Cambridge, MA 02139, USA

<sup>2</sup> Center for Advancing Materials Performance from the Nanoscale, State Key Laboratory for Mechanical Behavior of Materials, Xi'an Jiaotong University, Xi'an 710049, China

<sup>3</sup> Department of Materials Science and Engineering, Massachusetts Institute of Technology, Cambridge, MA 02139, USA

Supporting information to <https://doi.org/10.1007/s12274-019-2500-y>

The Electronic Supplementary Material includes further details on the dynamics of the stacking pattern transition, and the dielectric function of BBN.

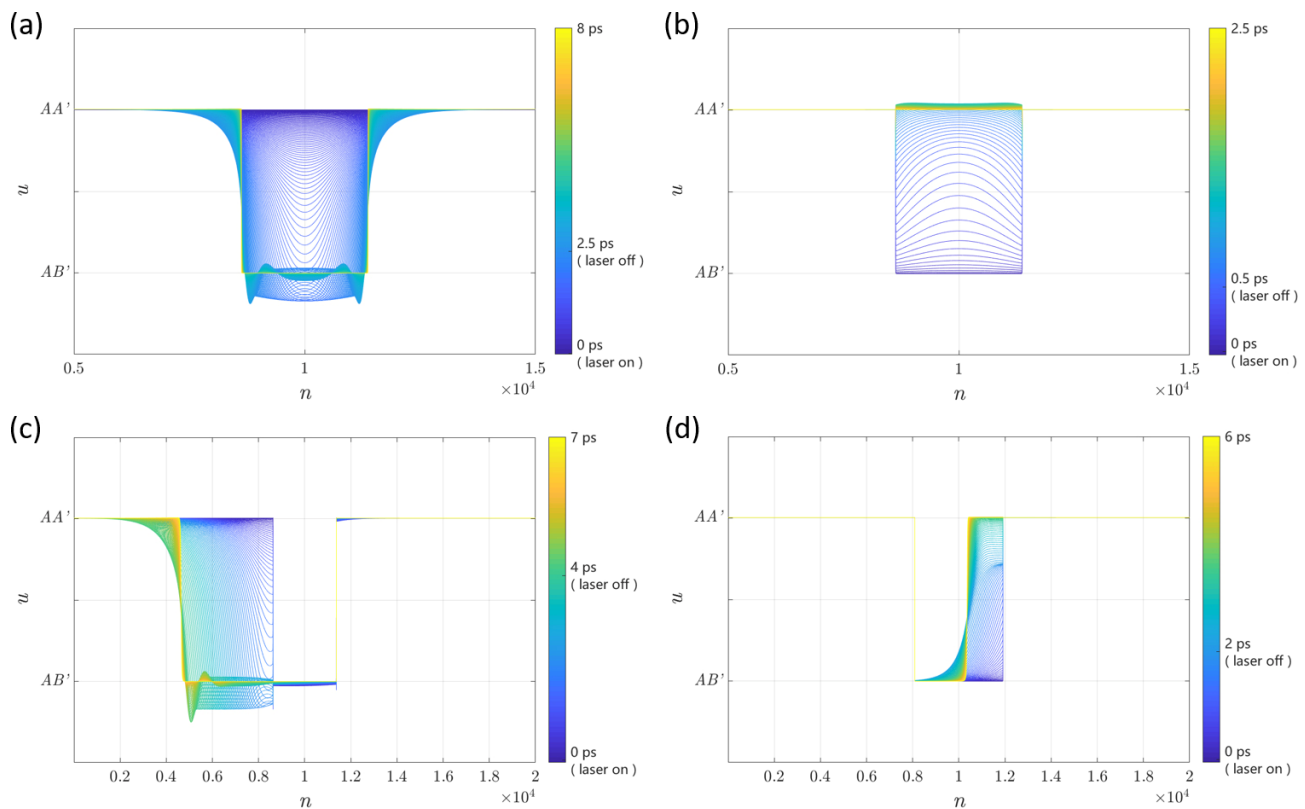


**Figure S1** Dynamics of the model system under laser illumination. The laser has the same time and spatial profile as that in Figure 3. But the force constant  $k$  in Eq. (3) is set as zero, thus the DW is thinner and should have  $\delta$  function (zero width) form as time approaches infinite. The DW, once formed, has no translational movement with time.

Address correspondence to [liju@mit.edu](mailto:liju@mit.edu)

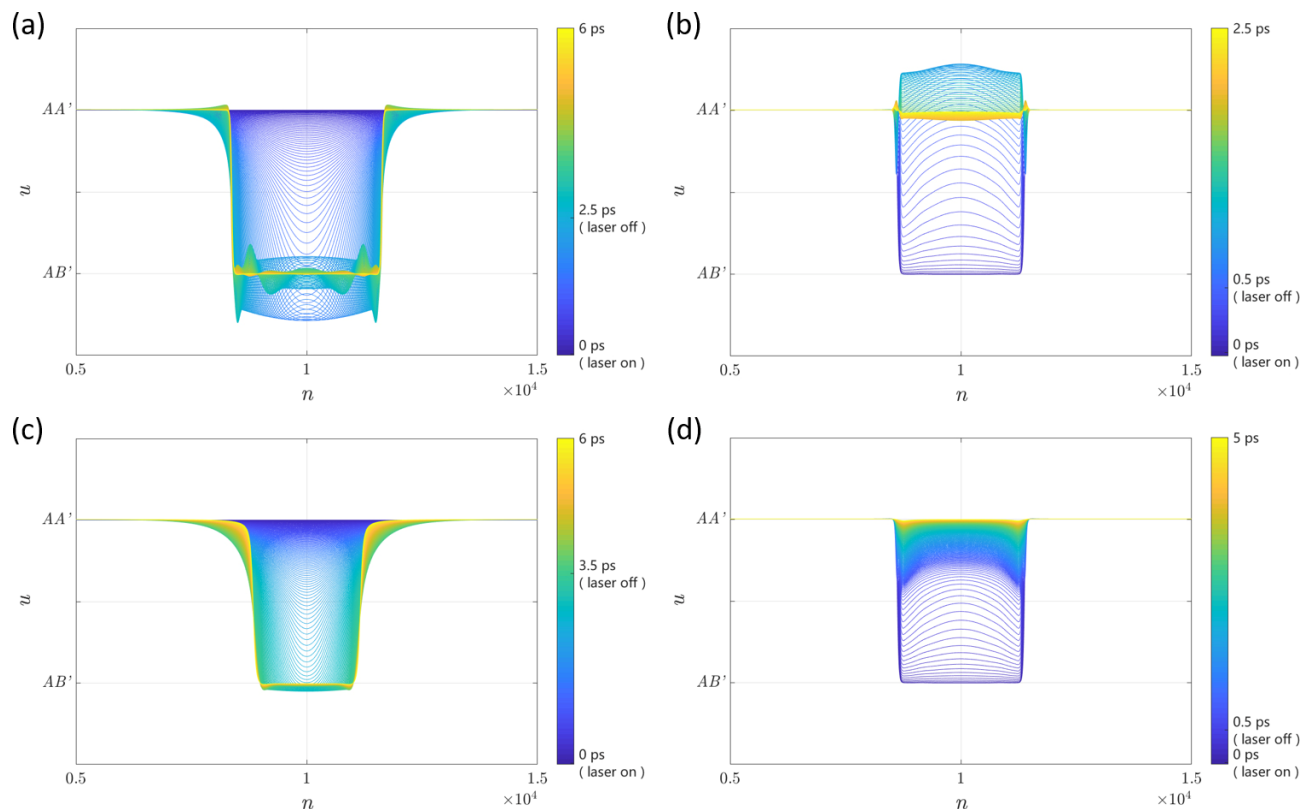


**Figure S2** Dynamics of the model system under laser illumination. The laser has the same time and spatial profile as that in Figure 3 in the main text. But in the upper panels, the dissipation rate  $\gamma$  is set as  $3 \text{ ps}^{-1}$ . The dynamics is faster but there are stronger oscillations around the energy minimum. In the lower panels  $\gamma$  is set as  $10 \text{ ps}^{-1}$ . The dynamics is slower, but there are no oscillations around the energy minimum. This corresponds to the over-damped regime. (a, c) writing AB' domain. (b, d) erasing AB' domain.

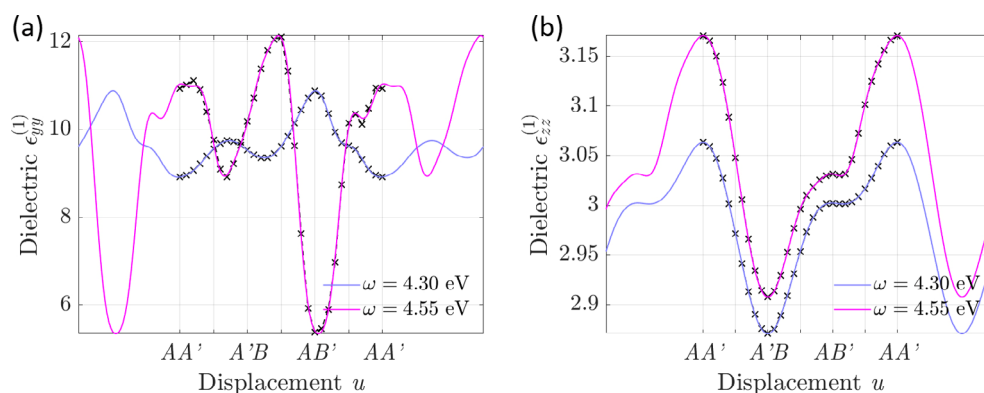


**Figure S3** The  $yy$  and  $zz$  components of Dielectric tensor at  $\omega = 4.3 \text{ eV}$  and  $4.55 \text{ eV}$ . The behavior of  $\epsilon_{yy}$  is similar to  $\epsilon_{xx}$  in Figure 2(c) of the main text, while  $\epsilon_{zz}$  is quite different.

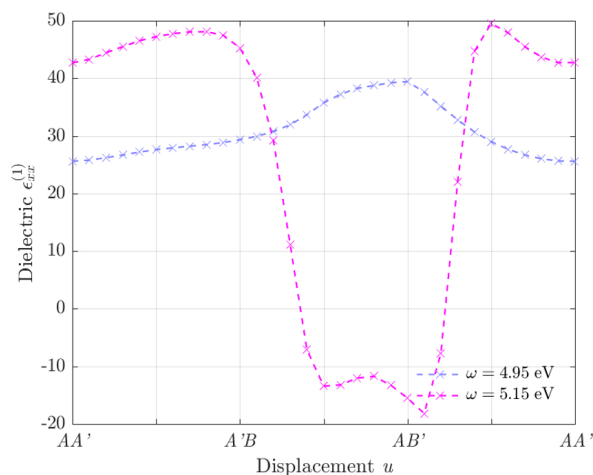


**Figure S4** Dielectric function  $\epsilon_{xx}^{(1)}(u, \omega)$  from GW-BSE calculation. Two selected frequency  $\omega = 4.95 \text{ eV}$  and  $5.15 \text{ eV}$  favor AB' and AA' stacking, respectively.